

Sensitivity Enhancement in Solid-State ^{13}C NMR of Synthetic Polymers and Biopolymers by ^1H NMR Detection with High-Speed Magic Angle Spinning

Yoshitaka Ishii, James P. Yesinowski,[†] and Robert Tycko*

Laboratory of Chemical Physics, National Institute of Diabetes and Digestive and Kidney Diseases, National Institutes of Health, Bethesda, Maryland 20892-0520

Received January 3, 2001

Indirect detection of ^{13}C and ^{15}N nuclear magnetic resonance (NMR) spectra through ^1H NMR signals offers large sensitivity advantages in studies of organic and biological molecules in solution and is almost universally employed.^{1–3} Although sensitivity enhancement by indirect detection was first demonstrated in NMR^{4–6} and nuclear quadrupole resonance^{7,8} of solids, direct detection has generally been preferred in solid-state NMR.⁹ This is because the broad ^1H NMR lines of organic solids negate sensitivity enhancement under the most common conditions. We have recently shown¹⁰ that substantial sensitivity enhancements can in fact be achieved by indirect detection in one-dimensional (1D) solid-state ^{15}N NMR spectroscopy of organic compounds and biopolymers under magic angle spinning (MAS) at speeds that greatly reduce the ^1H NMR line widths.^{10–12} Here we demonstrate the feasibility of sensitivity enhancement in solid-state ^{13}C NMR spectroscopy of general organic solids. We present experimental results both for the noncrystalline synthetic polymer poly(methyl methacrylate) (PMMA) and for the heptapeptide *N*-acetyl-Lys-Leu-Val-Phe-Phe-Ala-Glu-NH₂ ($A\beta_{16–22}$, representing residues 16 through 22 of the 40-residue Alzheimer's β -amyloid peptide¹³) in the form of amyloid fibrils. We report enhancements in both 1D and two-dimensional (2D) experiments. Extension to ^{13}C NMR, which forms the basis for many structural and dynamical studies in organic and biological systems, and to 2D spectroscopy significantly broadens the impact and generality of indirect detection methods in solid-state NMR.

The sensitivity enhancement factor ξ , defined as the ratio of frequency-domain signal-to-noise ratios for ^1H -detected and ^{13}C -detected measurements, is given by

$$\xi = \left(\frac{f^2 d}{\alpha}\right)^{1/2} \left(\frac{\gamma_{\text{H}}}{\gamma_{\text{C}}}\right)^{3/2} \left(\frac{W_{\text{C}}}{W_{\text{H}}}\right)^{1/2} \left(\frac{Q_{\text{H}}}{Q_{\text{C}}}\right)^{1/2} \frac{A_{\text{H}}}{A_{\text{C}}}$$

where γ is the magnetogyric ratio, W is the effective line width, Q is the quality factor of the sample coil, and A subsumes properties such as coil geometry, filling factor, receiver noise

[†] Permanent address: Chemistry Division, Naval Research Laboratory, Washington DC 20375-5342.

(1) Maudsley, A. A.; Müller, L.; Ernst, R. R. *J. Magn. Reson.* **1977**, *28*, 463–469.

(2) Müller, L. *J. Am. Chem. Soc.* **1979**, *101*, 4481–4484.

(3) Bax, A.; Griffey, R. H.; Hawkins, B. L. *J. Magn. Reson.* **1983**, *55*, 301–315.

(4) Bloembergen, N.; Sorokin, P. P. *Phys. Rev.* **1958**, *110*, 865–875.

(5) Hartmann, S. R.; Hahn, E. L. *Phys. Rev.* **1962**, *128*, 2042–2053.

(6) Mansfield, P.; Grannell, P. K. *J. Phys. C* **1971**, *4*, L197–L200.

(7) Redfield, A. G. *Phys. Rev.* **1963**, *130*, 589–595.

(8) Slusher, R. E.; Hahn, E. L. *Phys. Rev.* **1968**, *166*, 332–347.

(9) Pines, A.; Gibby, M. G.; Waugh, J. S. *J. Chem. Phys.* **1973**, *59*, 569–590.

(10) Ishii, Y.; Tycko, R. *J. Magn. Reson.* **2000**, *142*, 199–204.

(11) Filip, C.; Hafner, S.; Schnell, I.; Demco, D. E.; Spiess, H. W. *J. Chem. Phys.* **1999**, *110*, 423–440.

(12) van Rossum, B. J.; Boender, G. J.; deGroot, H. J. M. *J. Magn. Reson. Ser. A* **1996**, *120*, 274–277.

(13) Balbach, J. J.; Ishii, Y.; Antzutkin, O. N.; Leapman, R. D.; Rizzo, N. W.; Dyda, F.; Reed, J.; Tycko, R. *Biochemistry* **2000**, *39*, 13748–13759.

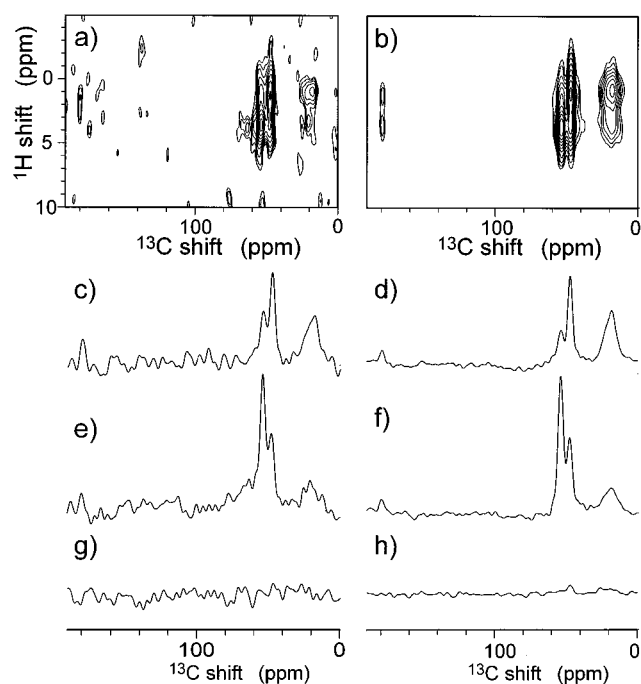


Figure 1. 2D $^{13}\text{C}/^1\text{H}$ heteronuclear correlation spectra of PMMA powder (9 mg, unlabeled) obtained with ^{13}C detection (a, c, e, g) and with ^1H detection (b, d, f, h). 1D slices are shown at ^1H shifts of 0.9 (c, d), 3.7 (e, f), and -3.5 ppm (g, h). See Figure 2 for ^{13}C assignments. The ^{13}C -detected spectrum is obtained with the rf pulse sequence $90^{\text{H}}_{\phi}-t_1^{\text{H}}-\text{CP}_x-t_2^{\text{C}}$. The ^1H -detected spectrum is obtained with the sequence $90^{\text{H}}_y-\text{CP}_x-t_1^{\text{C}}-90^{\text{C}}_{\phi}-\tau_d-90^{\text{C}}_y-\text{CP}_x-t_2^{\text{H}}$, where 90 is a $\pi/2$ pulse, CP is a 2 ms cross polarization period, t_1 is the evolution period, τ_d is a 5 ms period for dephasing of transverse ^{13}C magnetization and ^1H magnetization suppression (see text) and t_2 is the detection period. Superscripts H and C indicate ^1H and ^{13}C . Subscripts x , y , and ϕ indicate rf phases, with $\phi = x$ and y for quadrature detection in t_1 . ^1H rf field amplitudes are 71 kHz for CP and 8 kHz for decoupling during t_1^{C} or t_2^{C} . The ^{13}C rf field amplitude is swept from 50 to 30 kHz with a tangent shape during CP. No $^1\text{H}-^1\text{H}$ decoupling is applied during CP, so that each ^1H signal correlates with multiple ^{13}C signals. A total of 528 scans are acquired for each of spectra a and b. Lorentzian broadening of 390 Hz in the ^{13}C dimension and 770 Hz in the ^1H dimension is applied. Maximum t_1^{C} and t_2^{H} (or t_2^{C} and t_1^{H}) values are 1.28 and 0.65 ms, respectively.

figure, and lead loss.^{10,14} The symbols H and C refer to the ^1H and ^{13}C nuclei, f is the efficiency of polarization transfer between ^{13}C and ^1H spins, and d is the receiver duty factor for indirect detection (see below). When the ^1H -detected and ^{13}C -detected measurements have the same dimensionality, $\alpha = 1$. When the ^{13}C -detected measurement is 1D but the ^1H -detected measurement is 2D, $\alpha \approx 2\pi$ because of signal decay and the need for quadrature detection in the t_1 dimension.^{10,14} Typically, $A_{\text{H}}/A_{\text{C}} \approx 1$, $Q_{\text{H}}/Q_{\text{C}} \approx 2$, and $\gamma_{\text{H}}/\gamma_{\text{C}} = 3.98$, but in the absence of high-speed MAS or other line-narrowing techniques, $W_{\text{C}}/W_{\text{H}} < 0.01$ and consequently $\xi < 1$. Under MAS at sample rotation frequencies $\nu_{\text{R}} \geq 30$ kHz and ^1H NMR line widths are reduced approximately from 50 to 1 kHz. Then, for $W_{\text{C}} = 300$ Hz and $f = 0.5$, we find $\xi \approx 3.1(d/\alpha)^{1/2}$ and sensitivity enhancement appears possible.

Figure 1 compares 2D $^{13}\text{C}/^1\text{H}$ heteronuclear correlation (HETCOR) spectra of PMMA powder obtained with conventional ^{13}C detection and with ^1H detection. These spectra are acquired at 17.6 T (749.5 and 188.5 MHz ^1H and ^{13}C NMR frequencies) and

(14) Ernst, R. R.; Bodenhausen, G.; Wokaun, A. *Principles of Nuclear Magnetic Resonance in One and Two Dimensions*; Oxford University Press: Oxford, 1987; pp 148–153 and 349–354.

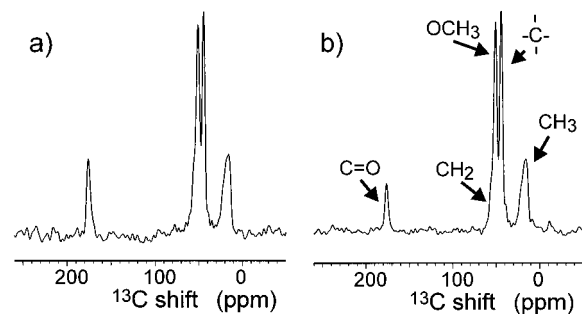


Figure 2. 1D ^{13}C NMR spectra of PMMA powder (4.5 mg, unlabeled) obtained with ^{13}C detection (a) and with ^1H detection (b). Total of 344 scans for each spectrum. Spectrum a is obtained in a 1D manner with CP and decoupling conditions as in Figure 1. Spectrum b is a single slice of a 2D spectrum obtained with the conditions in Figure 1b, but with a pulse spin locking (PSL) train applied in the t_2^{H} period and with $\tau_d = 4$ ms. The PSL train consists of one $6\ \mu\text{s}\ \pi/2$ pulse with phase x per sample rotation period. Complex ^1H signal points are sampled every $0.5\ \mu\text{s}$ during $14\ \mu\text{s}$ windows between PSL pulses.

$\nu_{\text{R}} = 31000 \pm 5$ Hz, with identical total acquisition times. Experimental ξ values are up to 3.3 for protonated carbon and 1.6 for the nonprotonated carbon signals. ^{13}C -detected HETCOR measurements^{15,16} are widely used as a means of resolving and assigning ^{13}C and ^1H chemical shifts in studies of synthetic polymers¹⁷ and biological compounds.^{12,18} The results in Figure 1 suggest that reductions in acquisition times by a factor of 10 may be possible in many cases through ^1H detection and high-speed MAS.

Figure 2 compares 1D ^{13}C NMR spectra of PMMA obtained at $\nu_{\text{R}} = 31250 \pm 5$ Hz and 17.6 T with conventional ^{13}C detection and with ^1H detection. In this case, because the ^{13}C -detected measurement is 1D but the ^1H -detected measurement is necessarily 2D, ξ is reduced by the factor $\alpha^{1/2}$. To compensate for this reduction, ^1H signals are detected with pulsed spin-locking (PSL),¹⁹ i.e., ^1H signals are sampled in windows between rotor synchronized radio frequency (rf) pulses that reduce the effective ^1H line width to roughly 50 Hz. Because of the finite pulse lengths and receiver dead time, the sampling windows comprise a fraction $d = 0.438$ of the total acquisition time. ^1H chemical shift information is lost under PSL, but this information is also absent in the 1D ^{13}C -detected measurement. For quaternary and protonated ^{13}C sites, $\xi \approx 2.5$ in Figure 2. For the carbonyl site, $\xi \approx 1.5$.

The PMMA samples in Figures 1 and 2 are not ^{13}C -labeled. A potential pitfall in ^1H -detected ^{13}C NMR measurements, especially at natural abundance, is the large “ t_1 noise”¹⁴ contributed by ^1H nuclei that do not participate in polarization transfer to ^{13}C nuclei. To obtain the sensitivity enhancements described above, we apply two $400\ \mu\text{s}$ rf pulses at the ^1H NMR frequency, with phases x and y and with amplitudes set to $\nu_{\text{R}}/2$ for rotary resonance recoupling,²⁰ during the ^{13}C dephasing period τ_d (see Figure 1 caption). These pulses destroy ^1H magnetization that would otherwise generate t_1 noise.

Figure 3 compares ^{13}C -detected and ^1H -detected $^{13}\text{C}/^1\text{H}$ HETCOR spectra of $\text{A}\beta_{16-22}$ fibrils obtained at $\nu_{\text{R}} = 31250 \pm 5$ Hz and 17.6 T. Ten percent of $\text{A}\beta_{16-22}$ molecules are ^{13}C -labeled at

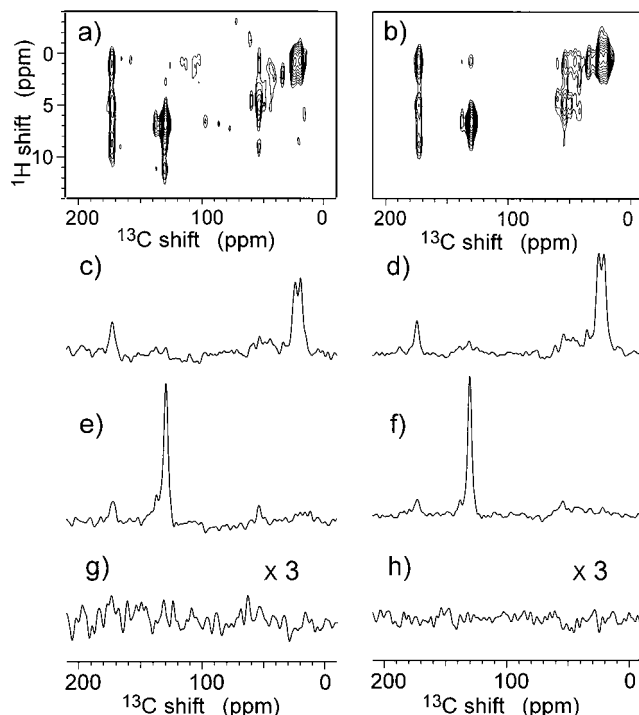


Figure 3. 2D $^{13}\text{C}/^1\text{H}$ heteronuclear correlation spectra of amyloid fibrils formed by the heptapeptide $\text{A}\beta_{16-22}$ (2 mg, lyophilized powder; peptides uniformly ^{13}C -labeled in the central five amino acid residues are diluted to 10% in unlabeled peptides) obtained with ^{13}C detection (a, c, e, g) and with ^1H detection (b, d, f, h). 1D slices are shown at ^1H shifts of 0.7 (c, d), 6.9 (e, f), and 13.0 ppm (g, h, vertical scale increased to show noise level). Experimental conditions are the same as in Figure 1 but $\tau_d = 6.5$ ms, maximum t_1^{C} and t_2^{H} (or t_2^{C} and t_1^{H}) values are 1.50 and 0.75 ms, and 9726 total scans per spectrum. Lorentzian broadening of 335 Hz in the ^{13}C dimension and Gaussian broadening of 675 Hz in the ^1H dimension are applied.

all carbon sites in the central five hydrophobic residues.¹³ ξ values are up to 2.4 for protonated and 1.8 for nonprotonated ^{13}C signals. Although the sharper ^{13}C lines in $\text{A}\beta_{16-22}$ fibrils lead to smaller ξ values than in Figure 1, these results still indicate a reduction of data acquisition time by a factor of 5.

The spectrum in Figure 3b provides new constraints on the structure of $\text{A}\beta_{16-22}$ amyloid fibrils. ^{13}C chemical shift assignments, initially determined from $^{13}\text{C}/^{13}\text{C}$ 2D exchange spectra,¹³ are confirmed by the present data. Additionally, ^1H chemical shifts determined from Figure 3b (5.1, 4.7, 5.1 ppm $^1\text{H}_{\alpha}$ shifts for Leu17, Val18, and Ala21, respectively, ± 0.3 ppm precision; 1.2 and 0.8 ppm $^1\text{H}_{\beta}$ shifts for Leu17 and Ala21) support a β -strand backbone conformation for the labeled residues.²¹ $^1\text{H}_{\alpha}$ (5.8 ppm) and $^1\text{H}_{\beta}$ (1.6 and 3.2 ppm) shifts for Phe residues and the $^1\text{H}_{\beta}$ (1.2 ppm) shift for Val18 are anomalous,²¹ possibly indicating intermolecular contacts of Phe residues and intermolecular or intramolecular contacts between Phe and Val residues in a laminated β -sheet structure.¹³

Acknowledgment. Supported in part by a grant to R.T. from the NIH Intramural AIDS Targeted Antiviral Program. Y.I. was supported by a postdoctoral fellowship from the Japan Society for the Promotion of Science.

Supporting Information Available: Table of chemical shifts from Figure 3 and expansion of Figure 3b with assignments (PDF). This material is available free of charge via the Internet at <http://pubs.acs.org>.

JA015505J

(21) Wishart, D. S.; Sykes, B. D.; Richards, F. M. *J. Mol. Biol.* **1991**, *222*, 311–333.

(15) Caravatti, P.; Braunschweiler, L.; Ernst, R. R. *Chem. Phys. Lett.* **1983**, *100*, 305–310.

(16) Roberts, J. E.; Vega, S.; Griffin, R. G. *J. Am. Chem. Soc.* **1984**, *106*, 2506–2512.

(17) White, J. L.; Mirau, P. A. *Macromolecules* **1994**, *27*, 1648–1650.

(18) Gu, Z. T.; Ridenour, C. F.; Bronnimann, C. E.; Iwashita, T.; McDermott, A. *J. Am. Chem. Soc.* **1996**, *118*, 822–829.

(19) Ostroff, E. D.; Waugh, J. S. *Phys. Rev. Lett.* **1966**, *16*, 1097–1098.

(20) Oas, T. G.; Griffin, R. G.; Levitt, M. H. *J. Chem. Phys.* **1988**, *89*, 692–695.